Available online at www.sciencedirect.com
SCIENCE DIRECT
Thermochimica Acta 438 (2005) 184–191
thermochimica acta
www.elsevier.com/locate/tca

On the thermal stability of $LiPF_6$

Ella Zinigrad [a], Liraz Larush-Asraf [a], Josef S. Gnanaraj [b], Milon Sprecher [a], Doron Aurbach [a,*]

[a] *Department of Chemistry, Bar-Ilan University, Ramat-Gan 52900, Israel*
[b] *Chemical Engineering, Worcester Polytechnic Institute, 100 Institute Road, Worcester, MA 01609, USA*

Received 24 July 2005; accepted 3 September 2005
Available online 5 October 2005

Abstract

The results of a comprehensive study of the thermal stability of the salt $LiPF_6$, using both accelerating rate (ARC) and differential scanning (DSC) calorimetry, are presented. Pressure monitoring during ARC experiments permits also the study of endothermic processes. The origins of apparently inconsistent results and conflicting interpretations in previous reports in the literature are explicated. In a confined volume, $LiPF_6$(s) melts reversibly at 467 K with a heat of melting of $2.0 \pm 0.2\,kJ\,mol^{-1}$. Reversible decomposition to PF_5(g) and LiF(s) commences with melting, but the autogenic development of PF_5(g) pressure makes the temperature profile of decomposition a function of volume and sample size. The heat of this reaction at constant volume, ΔU_r, as determined by a variety of methods is in the range $60 \pm 5\,kJ\,mol^{-1}$, and is approximately temperature independent in range 490–580 K.

Keywords: ARC; DSC; Thermal decomposition; Hexafluorophosphate

1. Introduction

There is no doubt that the recent development and commercialization of high energy density, rechargeable Li-ion batteries is one of the most important successes in modern electrochemistry. These battery systems are conquering the market, and their range of application continues to expand. In the meantime, a huge amount of scientific work is being devoted to this field by thousands of research groups throughout the world, because of the complexity of these systems, whose operation involves highly complicated Li intercalation reactions, interfacial charge transfer reactions, passivation and corrosion phenomena, and simultaneous surface and bulk side reactions. At present, all the commercial Li-ion batteries comprise electrolyte solutions based on a $LiPF_6$ salt and alkyl carbonate solvents. Despite its reactivity with Li-C anodes and Li_xMO_y cathodes (M = transition metals such as Mn, Ni, Co, etc.), $LiPF_6$ was chosen as a compromise because its nonaqueous solutions are highly conductive, and it is less dangerous and poisonous than other possible suitable salts such as $LiClO_4$ or $LiAsF_6$ [1,2]. In recent years, calorimetric tools such as differential scanning calorimetry (DSC) and accelerating rate calorimetry (ARC) were widely used in this field in order to study the thermal stability of Li batteries and their components [3,4]. The crucial role of $LiPF_6$ in the determination of the thermal behavior of these systems has been clearly demonstrated. Consequently, there is no doubt that the thermal behavior of $LiPF_6$ itself is interesting and important, and thus deserves special attention.

Indeed, the thermal stability of $LiPF_6$ has been studied in recent years using various methods and approaches [5–9]. These included calorimetric measurements at constant volume [6,8,9] constant pressure [5,6], dynamic or isothermal conditions, differential scanning calorimetry with and without gas removal, in closed or open crucibles, and thermogravimetric analysis (TGA) under nitrogen flow [5]. It was found that $LiPF_6$ is not stable at elevated temperatures and decomposes to LiF and PF_5, demonstrating one [6] or two [8] endothermic peaks in DSC at constant volume, and more that two peaks [6] at normal pressure. Since the thermal decomposition of $LiPF_6$ is accompanied by the development of PF_5 gas, the onset of these endothermic processes depends on the test conditions. In an open crucible under nitrogen flow at atmospheric pressure, the isothermal TGA measurements show a weight loss related to only one process at temperatures as low as 343 K [5]. In closed crucibles during

* Corresponding author. Fax: +972 3 5351250.
E-mail address: aurbach@mail.biu.ac.il (D. Aurbach).

0040-6031/$ – see front matter © 2005 Elsevier B.V. All rights reserved.
doi:10.1016/j.tca.2005.09.006

DSC measurements, the onset of the first endothermic process is close to 468 K [6,8,9]. It appears as a peak and is reversible [6,8].

Though the endothermic decomposition of $LiPF_6$ at elevated temperatures has been intensively explored, the observations reported in the literature regarding the onset of its decomposition and the dependence of heat flow on T in DSC experiments are not consistent. There is furthermore no one clear and unified explanation for the endothermic behavior observed. Thus, some [8] have observed a first endothermic onset at 453 K in sealed crucibles, and have suggested that the peak is connected to the melting point of the salt. Du Pasquir et al. [9] obtained the first endothermic peak near 463 K but did not discuss it. The second endothermic peak in their measurements was attributed to the melting point of $LiPF_6$, but the onset was observed at about 513 K. Gavritchev et al. [6] attributed the first endothermic peak at about ~468 K in $LiPF_6$/DSC measurements to the decomposition of $LiPF_6$, and not to any phase transition. In experiments with sealed crucibles, they did not find an additional endotherm below 513 K. However, it was shown [6] that the decomposition of $LiPF_6$, when it occurs, is suppressed by the autogenic development of PF_5 pressure.

The present work aims at providing a better and more complete picture of the thermal behavior of $LiPF_6$, and to explain relevant calorimetric responses. To this purpose, we used two separate tools:

1. DSC measurements of hermetically sealed crucibles loaded with different amounts of $LiPF_6$.
2. ARC measurements of $LiPF_6$ with a special arrangement in which the pressure developed is rigorously measured, in addition to the temperature changes.

2. Experimental

An accelerating rate calorimeter from Arthur D Little Inc., Model 2000, and a differential scanning calorimeter from Mettler Toledo Inc., Model DSC 822, were used.

In the ARC tests about 2 g of salt were loaded into the titanium flask (8.2 ml volume) in an argon filled glove box (VAC Inc.) and were transferred to the ARC under a purified Ar atmosphere. The salt was heated from 313 to 548 and 623 K, respectively, in 5 °C increments at the rate of 2 °C min^{-1} in the search for self-heating at a sensitivity threshold of 0.02 °C min^{-1}. The controller was programmed to wait 15 min for the sample and the calorimeter temperatures to equilibrate, and then to search during 20 min for a temperature increase of 0.02 °C min^{-1}. After the ARC experiments, the reaction vessel (a titanium flask) was cooled with liquid nitrogen until the pressure was slightly above the atmospheric pressure. The gas was then released through a specially designed high-pressure valve.

DSC tests were conducted in high pressure, gold-plated stainless steel crucibles 30 μl in volume, over a temperature range of from 303 to 623 and 673 K, respectively. The crucibles were filled with 1–7 mg of the salt, and then sealed in a glove box under an argon atmosphere. The heating/cooling rates were 0.5, 1, 2, 5, 8, 10, 20 and 30 K min^{-1}.

The XRD patterns of the solid product were measured using the Advanced D8 diffractometer from Bruker Inc. The patterns measured at RT showed typical peaks of $LiPF_6$ and LiF (well-known XRD) patterns.

3. Results and discussion

3.1. ARC measurements

Fig. 1 shows temperature and pressure changes (in time) measured during ARC experiments with 1.9 g of $LiPF_6$ heated up to 548 K. The ARC construction and software is designed to study exothermic processes by temperature changes, but not endothermic processes. Nevertheless, by a thorough examination of the pressure changes during ARC experiments, and by careful analysis of the temperature behavior, it is possible to use ARC for the study of endothermic processes as well.

Typical results from these ARC measurements are presented in Fig. 1a and b. Fig. 1b enlarges the results related to the 450–490 K temperature range. The arrow in Fig. 1b shows an unusual temperature drop of 2.09 °C during a waiting and searching stage, between 460 and 465 K. There were no significant pressure changes in this range. The normal temperature decrease in all the other steps was only by 0.65–1.25 °C. This abnormal phenomenon can be explained only by an endothermic process (melting), which was also observed by DSC measurements, as discussed below. In the following steps, the decompo-

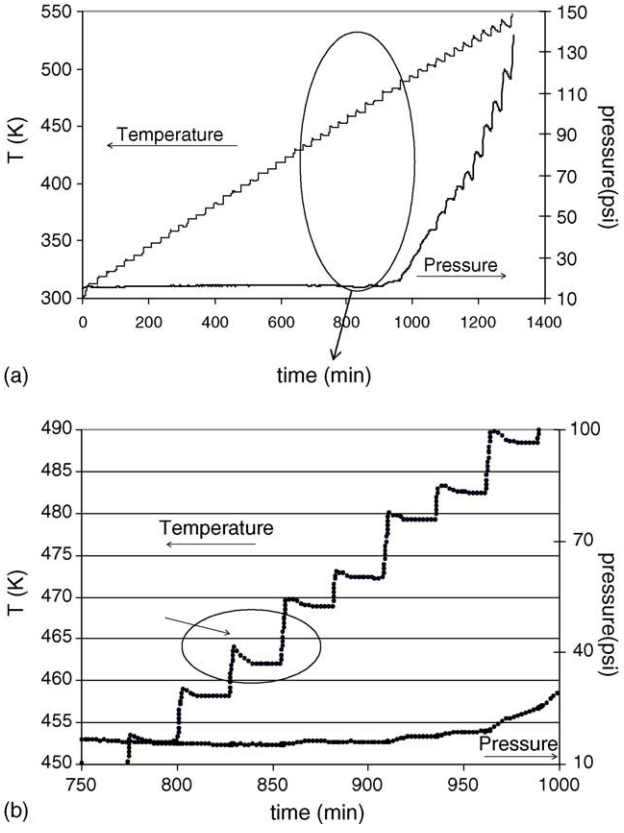

Fig. 1. (a) Typical ARC response during heating process of $LiPF_6$. (b) The chart emphasizes the behavior in the temperature range 450–490 K.

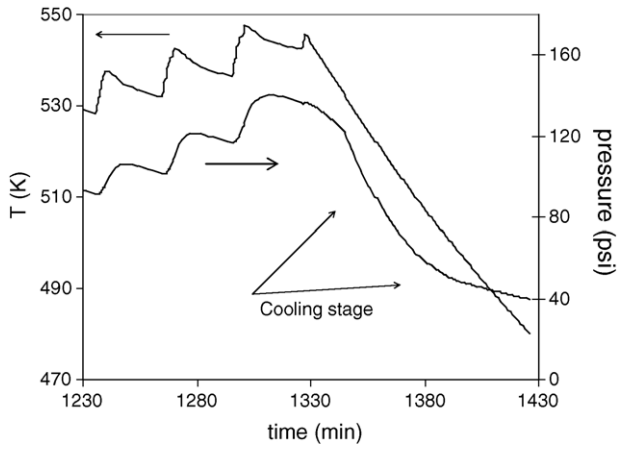

Fig. 2. In each step of the ARC measurements, an equilibrium pressure is measured, T, P vs. t.

sition of $LiPF_6$ is accompanied by gas evolution:

$$LiPF_6\,(\text{liquid}) \leftrightarrow LiF\,(\text{solid}) + PF_5\,(\text{gas}) \quad (1)$$

The heat of the endothermic processes cannot be calculated by ARC measurements.

The pressure changes in the cooling stage is presented in Fig. 2.

The significant pressure growth that starts above 473 K is, of course, related to the salt decomposition and PF_5 formation (Eq. (1)). The pressure measured at 548 K was 137 psi. The amount of salt decomposed could be calculated by the measurements of pressure, provided that the equation of the state of the gas is known (e.g., for a perfect gas, $PV = nRT$, where n is the number of gas moles). Real gases of course deviate from the perfect gas law. The compression factor Z ($Z = PV_m/RT$) can be used in the framework of a virial equation of state:

$$PV_m = RT\left(1 + \frac{B}{V_m} + \frac{C}{V_m^2} + \cdots\right), \quad (2)$$

where B and C are the second and the third virial coefficients, and V_m is the molar volume. The compression factor Z can be defined as the ratio:

$$Z = \frac{V_m}{V_m^0}, \quad (2a)$$

where V_m^0 is the molar volume of a perfect gas.

Based on this equation, the measured pressure values can be used for calculating V_m, and hence, n, if V is known. In general, $C/V_m^2 \ll B/V_m$, and hence the third term in the equation above, can be neglected. The virial coefficients depend of course on the temperature.

In our case, the number of $LiPF_6$ moles in the sample, and hence the maximal moles of PF_5 gas formed, are:

$$n_{LiPF_6} = \frac{m}{M} = \frac{1.9}{152} = 12.5\,\text{mmol}, \quad (3)$$

where $m = 1.9$ g is the weight of the sample, and $M = 152$ the molecular mass of $LiPF_6$.

This means that for the ARC vessels' volume, which is 8.2 cm^3, the limit of the molar volume of the PF_5 gas that can be formed (i.e., due to the full decomposition of the salt) is equal to $8.2/0.0125 = 656\,cm^3\,mol^{-1}$. The highest value of the second virial coefficient B at 600 K, based on the Handbook of American Institute of Physics [10] for a heavy gas such as Xe, is $19.6\,cm^3\,mol^{-1}$. If we presume that the coefficient B at 513 K taken for heavy gases is, for example, $40\,cm^3\,mol^{-1}$, which should be considered as an exaggeration for our case, we obtain:

$$\frac{B}{V_m} = \frac{40}{656} = 0.061. \quad (4)$$

In our case, the molar volumes of the PF_5 gas produced are relatively high, and thereby, the second term in Eq. (2) is relatively small. Hence, the real gas equation of state converges to that of an ideal gas.

The number of moles of the gas (including both Ar and PF_5) in the vessel's volume of 8.2 cm^3 at 548 K and at 137 psi (9.32 atm) (Fig. 2) is equal to:

$$n = \frac{PV}{RT} = \frac{9.32 \times 0.0082}{0.082 \times 548} = 1.7\,\text{mmol}, \quad (5)$$

where $R = 0.082$ L atm mol^{-1} K^{-1}.

The initial pressure of Ar in the bomb is 1 atm, and the salt volume is: $V = \frac{m}{\rho} = \frac{1.9}{2.838} = 0.67 cm^3$, where $\rho = 2.838\,cm^3$ is the density of $LiPF_6$ [11].

Therefore the amount of Ar (moles) in the bomb is:

$$n_{Ar} = \frac{PV}{RT} = \frac{1 \times (0.0082 - 0.00067)}{0.082 \times 298} = 0.31\,\text{mmol}. \quad (6)$$

The pressure reduction due the cooling of the vessel from 548 to 483 K should have been less than what was actually observed. 1.7 mmol of gas occupying a volume of 8.2 cm^3 results at 483 K:

$$P = \frac{nRT}{V} = \frac{0.0017 \times 0.082 \times 483}{0.0082} = 8.21\,\text{atm} = 120.7\,\text{psi}. \quad (7)$$

However, the measured pressure at 483 K was only 41 psi. This difference is due to the reverse reaction 1. On the other hand, the pressure actually measured at 483 K is too high for a case where all the PF_5 reacts with LiF to form $LiPF_6$. At 483 K, the partial pressure expected for the argon in the reaction vessel should not be higher than that for 0.31 mmol of gas:

$$P = \frac{nRT}{V} = \frac{0.00031 \times 0.082 \times 483}{0.0082} = 1.49\,\text{atm} = 22\,\text{psi}. \quad (8)$$

We should note that the above evaluations can suffer the following errors:

1. The titanium bomb expands upon heating and hence its volume is also temperature dependent.
2. The masses of the solid LiF and liquid $LiPF_6$ also occupy some volume. We do not have information on the specific density of liquid $LiPF_6$.

In any event, taking into account the specific density of solid $LiPF_6$ and LiF (2.838 and 2.635 g cm^{-3}, respectively) and the thermal expansion of Ti, $\alpha_l = 8.6 \times 10^{-6}\ K^{-1}$, the errors in the above calculations are estimated to be less then ±1%.

Hence, the difference of 19 psi between what was measured and the partial pressure of argon is due to the remaining PF_5 that did not react with LiF to re-form $LiPF_6$. This residual gas corresponds in amount to the LiF that we found by XRD analysis showed the presence of the LiF [11] in the solid mixture remaining after the heating and cooling cycle of $LiPF_6$. This finding correlates with the conclusions from the DSC measurements (see next section) that show that the PF_5 and LiF formed by thermal decomposition of $LiPF_6$ at elevated temperatures in closed vessels (as is the case for the ARC and DSC measurements reported herein), did not, when cooled, recombine in entirety to form the original amount of $LiPF_6$. This is presumably because upon cooling, the first-formed $LiPF_6$ is a liquid that covers the remaining LiF crystallites. For these to react, the PF_5 must diffuse through the layer of $LiPF_6$ whose thickness increases as the reverse reaction proceeds. A time much longer than that available during cooling in these measurements is needed for all the PF_5 to recombine with the coated LiF.

During heating in the ARC experiments, we measured the equilibrium pressure at the end of the searching time, and at each temperature range, we waited for a time sufficient to allow the compounds in the reaction vessel to equilibrate (Fig. 2). We also showed that in these experiments we could use the approximations of a perfect gas for the pressure values that we measure. If $LiPF_6$ and LiF are assumed to be pure phases in the temperature ranges measured (i.e., there is no unreacted PF_5 or LiF in the molten $LiPF_6$), then the pressure of the PF_5 measured at different temperatures (total pressure measured minus the partial pressure of argon) would reflect the equilibrium constant of the decomposition reaction at each temperature (K_p). P_{PF5} versus T is plotted in Fig. 3a and $\ln P(PF_5)$ versus $1/T$ is plotted in Fig. 3b (for ARC experiments with 1.9 g of $LiPF_6$ heated up to 623 K). The relatively good linear correlation thus obtained, allows the calculation of an approximate heat of reaction at constant volume (ΔU_r) using a non-calorimetric method by using the integral form of the van't Hoff isochoric equation, $\ln K = -\Delta U_r/RT - \text{const.}$ ΔU_r – nearly invariant in the temperature range measured (503–578 K) – was found to be $64.9 \pm 0.3\ kJ\ mol^{-1}$ e. This value is close to that reported by Gavritchev et al. [6] as ΔH ($69\ kJ\ mol^{-1}$) for the same reaction (Eq. (1)) in the same temperature range, carried out under constant pressure conditions. The difference, $\Delta H - \Delta U_r$, is very close to RT ($n = 1$), where T is the average temperature in the relevant temperature range.

3.2. DSC measurements

Figs. 4 and 5 present typical DSC heating/cooling curves for several samples of $LiPF_6$ of different weight, including curves for second and third consecutive heating/cooling cycles (Fig. 5). These curves show well-defined melting/crystallization peaks at 467.4 ± 0.4 K (endothermic) and 460.2 ± 0.4 K (exothermic), respectively (Tables 1 and 2). In multiple cycles on the same sample, the $LiPF_6$ melting temperature in the second cycle is slightly below that in the first cycle.

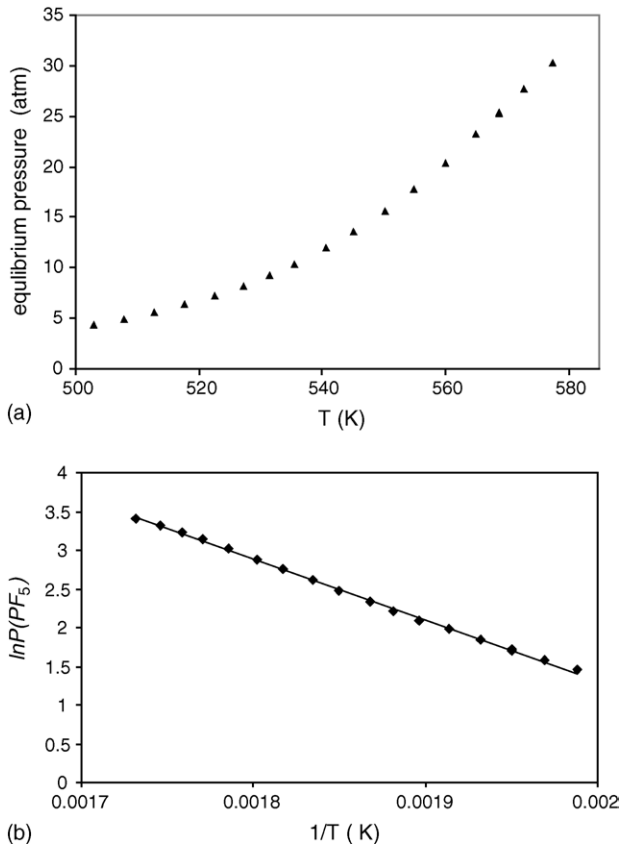

Fig. 3. The equilibrium pressure of PF_5 that is formed by thermal decomposition of $LiPF_6$, [$LiPF_6$ (l) ↔ LiF (s) + PF_5 (g)], as a function of temperature related to the ARC measurements in Fig. 2: (a) P_{eq}. vs. T; (b) $\ln(P_{PF5})$ vs. $1/T$.

The melting heat of $LiPF_6$ measured in the temperature interval 443–473 K is $2.02 \pm 0.18\ kJ\ mol^{-1}$.

In order to understand the nature of the endothermic process measured by DSC at 468 K, we conducted experiments in which $LiPF_6$ was heated in closed quartz ampoules, whose temperature was monitors. We observed visual changes in the morphology of the heated samples during the heating process. At temperature close to 467 K, we could clearly observe morphological changes that looked like liquid layers that were formed and covered the solid crystals of the salt. We could also observe gas formation and some bubbling. Thereby, we concluded that the endothermic process at 467 K is melting of $LiPF_6$, which is followed by its decomposition from the liquid state, thus forming solid LiF crystals (clearly visible in these experiments) and PF_5, as heating proceeds. In any complete heating-cooling cycle, the total heat of crystallization was always less than the heat of melting. However, the ratio of the two is a function of the mass of the sample (see Fig. 6a). Thus, as noted in the discussion of the ARC results, the reformation of $LiPF_6$, which decomposed to PF_5 + LiF upon heating, is never fully completed upon cooling. From the ratio of the heat of crystallization to that of melting in the same cycle one can calculate the fraction of the original $LiPF_6$ which has been reformed as well as the amount of residual LiF in the that experiment. From the data in Fig. 6a, it may be seen that in these

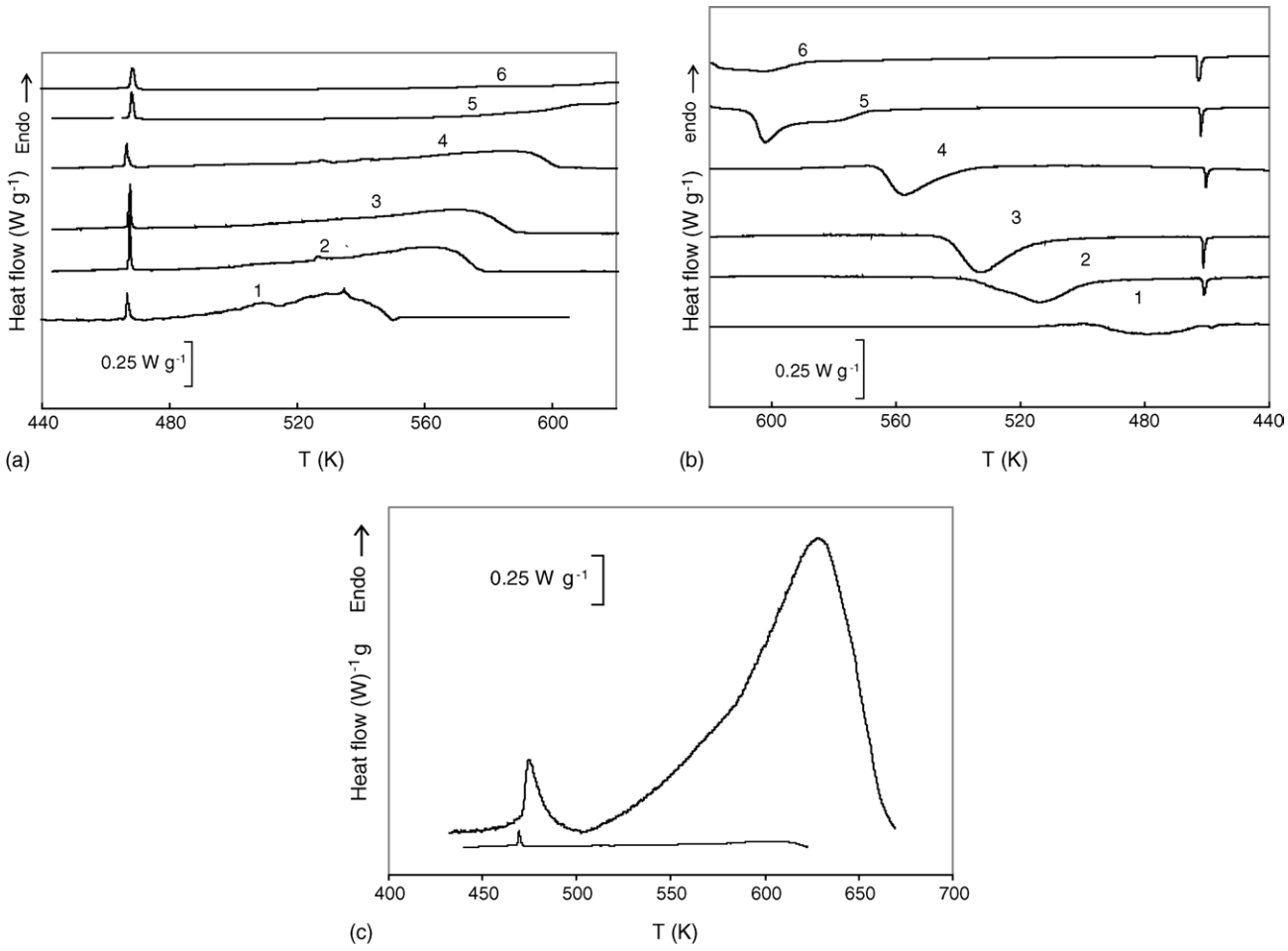

Fig. 4. DSC curves of $LiPF_6$ samples at heating rate/cooling rate of 1 K min^{-1}, weighing 1–1.074 mg, 2–2.676 mg, 3–3.645 mg, 4–5.862 mg, 5–13.875 mg, 6–26.700 mg: (a) heating; (b) cooling; (c) lower curve–11.577 mg, upper curve–11.078 mg at heating rate of 1 and 20, respectively.

experiments only 13–50% of the original $LiPF_6$ was reformed, depending on the size of the sample. Fig. 6b presents the data in terms of the mass of residual LiF as a function of mass of the original $LiPF_6$ sample.

Upon the first heating at the lower rate, the endothermic decomposition process is not separated from melting and the shape of the curves and peak depends on the mass of the sample (Figs. 4a and 5). Fig. 4c shows typical DSC curves at higher heating rates.

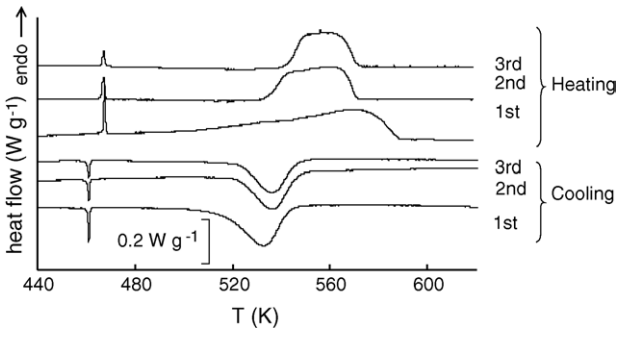

Fig. 5. The first, second and third DSC consecutive heating and cooling curves of a $LiPF_6$ sample, weighing 3.645 mg.

Fig. 7 demonstrates that the greater the sample mass, the higher the peak temperature of the endothermic decomposition. A rationalization of this finding will be presented below. It should however be noted at this point that the sample mass that Gavritchev et al. [6] used, corresponds to ~20 mg in our tests. It is clear from Fig. 6 that a decomposition peak of 20 mg (132 μmol) $LiPF_6$ in a sealed crucible, such as we used, is at temperature higher than 513 K. Gavritchev et al. [6] worked with sealed crucibles in the range 298–513 K. It is clear therefore why they did not observe a decomposition peak, and detected only the reversible melting/crystallization peak near 463 K, which they misidentified.

Upon repeated cycling of the same sample at the heating rate 1 K min^{-1} the melting and the decomposition peaks are separated and the decomposition peaks in the subsequent heating cycles become progressively narrower and more symmetrical (Fig. 5).

Distinguished separation between the melting and the decomposition peaks upon the first heating was observed at high heating rates. Fig. 4c shows DSC curves of $LiPF_6$ samples at heating rates of 1 and 20 K min^{-1}. The masses of the samples are very close as indicated in Fig. 4c. As the rate increases from 1 up to 20 K min^{-1}, the melting peak shifts to higher temperatures by

Table 1
Parameters related to the $LiPF_6$ melting and decomposition, appearing in the DSC curves at heating rate of 1 K min^{-1}

No.	Weight (mg)	Weight (μ mol)	Melting peak onset (K)	Melting peak temperature (K)	ΔU_r of melting (kJ mol^{-1})	Decomposition peak temperature (K)	ΔU_r of decomposition (kJ mol^{-1})
1	1.074	7.07	467.46	467.92	2.26	535.70	50.54
2	1.453	9.56	467.23	468.07	2.15	520.00	54.88
3	2.676	17.61	467.01	467.36	2.32	562.50	61.75
4	2.386	15.70	466.21	466.57	2.12	564.30	46.05
5	3.645	23.98	466.84	467.48	2.35	570.40	65.07
6	3.696	24.32	466.51	466.90	1.97	574.30	57.39
7	5.862	38.57	467.06	467.78	1.62	557.42	54.91
Average			466.90 ± 0.33	467.44 ± 0.42	2.02 ± 0.18		55.79 ± 4.80

ca. 7 K, while the shift of decomposition peak is ca. 24 K. Comparing DSC curves obtained at different heating rates (Fig. 4a and c) shows that the first endothermic peak does not relate to the consequent endothermic decomposition. The melting heat of $LiPF_6$ measured in the temperature range 445–503 K at heating rate 20 K min^{-1} is 1.8 kJ mol^{-1}. This result correlates with the average value measured at a heating rate of 1 K min^{-1} that was estimated without deconvolution between the melting and the decomposition peaks (Table 1).

The cooling curves show the exotherm peaks resulting from the reformation of $LiPF_6$ from PF_5 and LiF. These are much more symmetric in shape than the respective endotherm peaks upon heating, both in the case of sample cycled once (Fig. 4b) and in the case of repeated cycling (Fig. 5). As for the endotherms, so also for the exotherms, their onset and peak temperature are function of the mass of the original $LiPF_6$ samples (Figs. 4b and 8); the larger the sample, the higher the temperatures. For each sample the quantity of heat absorbed upon decomposition of $LiPF_6$ was significantly larger than that released during $LiPF_6$ reformation upon cooling, and the ratio $Q_{reformation}/Q_{decomposition}$ is dependent on the mass of the sample. This is in keeping with the conclusion presented above regards incomplete reformation of $LiPF_6$ upon cooling. In fact the extent of reformation calculated for any sample from $Q_{reformation}/Q_{decomposition}$ corresponds to the extent calculated from $Q_{crystallization}/Q_{melting}$. This is shown in Fig. 6a.

The rationalization of the above findings is of necessity qualitative since quantitative data for key phenomena, such as the equilibrium constant for Eq. (1) as a function of temperature, are unknown, as are the solubility of PF_5 and LiF in liquid $LiPF_6$. The latter solubility is probably very small, in keeping with its high melting point (1143 K). The endothermicity measured upon heating above 473 K reflects not only the net heat of decomposition of $LiPF_6$ in the liquid phase (and the specific heats of the components). It also includes the outcome of secondary thermal processes such as the exothermic formation of a crystalline LiF solid phase (possibly via an amorphous stage), and the separation of PF_5 bubbles into the gas phase. These may be accompanied by supersaturation phenomena. It is therefore not surprising that the first cycle DSC heating curves frequently show poor reproducibility. A specific example is curve 1 in Fig. 4a, exemplifying the finding for a very small sample (1.074 mg). Two poorly resolved peaks appear. The existence of a second peak cannot be attributed to the further decomposition of PF_5 to $PF_3 + F_2$, since the equilibrium constant for this reaction at this temperature is negligible ($\sim 10^{-55}$) [10]. Rather it is suggested that in the case of such a small sample, disconnected micro droplets are formed upon $LiPF_6$ melting, and these suffer different secondary behavior.

In a sealed DSC crucible of given volume the larger the $LiPF_6$ sample, the smaller the fraction which must decompose to reach equilibrium pressure of PF_5 and repress further net decomposition at that temperature. To continue, and eventually attain substantially complete decomposition as per Eq. (1), the temperature must be progressively raised. This explains the shift of the endotherm peak covering complete decomposition to higher temperatures as the mass of the sample is increased (Fig. 4a). Similarly, upon cooling the greater PF_5 pressure leads to the

Table 2
Parameters related to the $LiPF_6$ reformation and crystallization, appearing in the DSC curves at heating/cooling rate of 1 K min^{-1}

No.	Weight (mg)	Weight (μ mol)	Reformation peak onset (K)	Reformation peak temperature (K)	ΔU_r of reformation (kJ mol−1)	Crystalization peak onset (K)	Crystalization peak temperature (K)	ΔU_r of crystallization (mJ)
1	1.074	7.07	496.00	479.98	68.55	460.73	459.70	2.14
2	1.453	9.56	503.26	487.00	49.62	461.06	460.14	6.36
3	2.676	17.61	525.96	513.89	69.41	461.49	460.89	14.14
4	2.386	15.70	522.47	510.52	63.91	460.40	459.61	16.00
5	3.645	23.98	542.79	532.81	66.91	461.45	461.04	25.04
6	3.696	24.32	541.95	532.90	59.03	460.45	460.09	22.46
7	5.862	38.57	573.59	557.42	45.18	460.76	460.41	30.00
Average					60.37 ± 7.80	460.90 ± 0.36	460.27 ± 0.43	

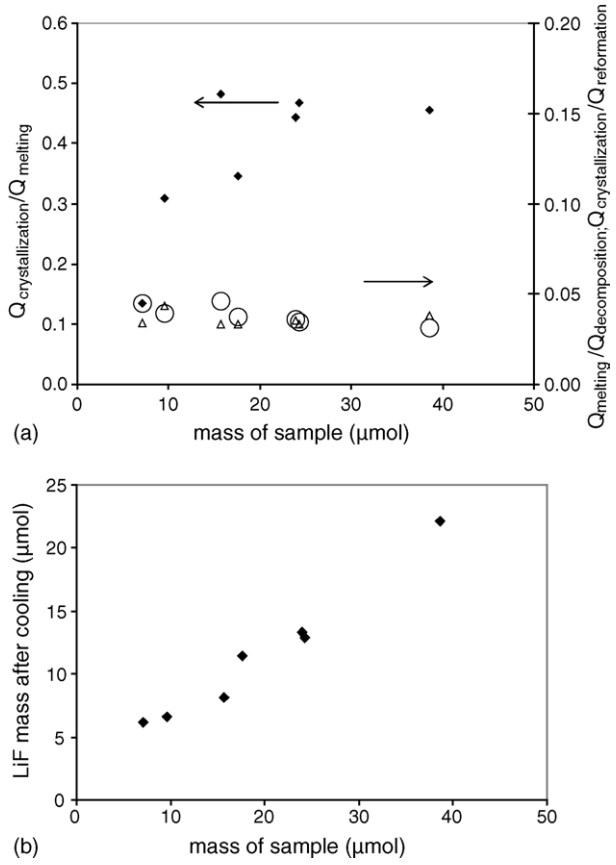

Fig. 6. (a) The extent of the reverse $LiPF_6$ reformation as a function of the samples' mass in DSC experiments: (♦) crystallization heat/melting heat; (Δ) crystallization heat/heat of reformation reaction; (◯) melting heat/heat of decomposition reaction. (b) The LiF mass that remained after cooling as a function of the samples mass (calculated from the DSC measurements).

onset of the exotherm ($LiPF_6$ reformation) at a higher temperature, the larger the sample of $LiPF_6$, which has been decomposed (Figs. 4b and 8).

Since the reformation of $LiPF_6$ upon cooling is incomplete, in repeated cycling of the same sample the LiF crystallites remaining from the previous cycle act as seed for the crystallization of LiF (and possibly as catalyst for release of PF_5 gas) formed by $LiPF_6$ decomposition in the subsequent cycle.

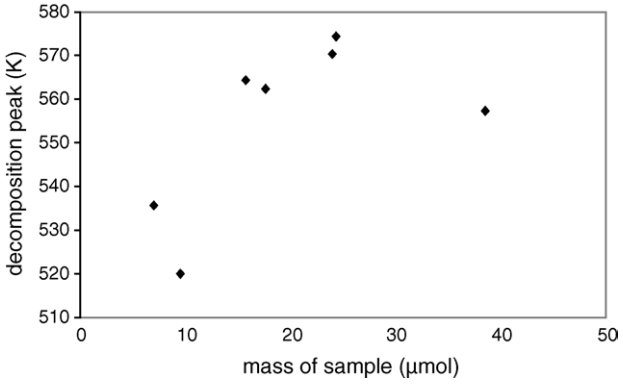

Fig. 7. The dependence of the endothermic decomposition peak's position on the sample mass in DSC experiments.

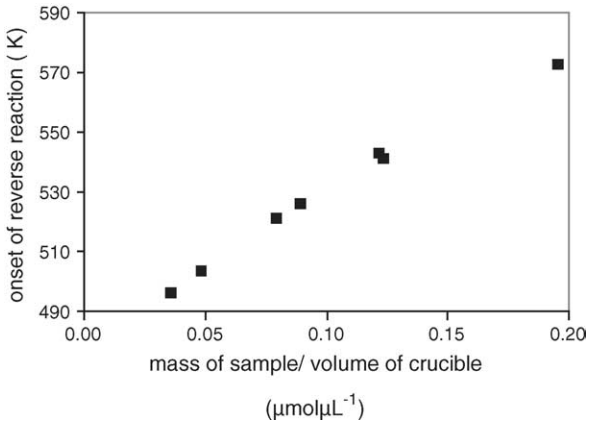

Fig. 8. The dependence of the onset of the reverse reaction $LiF + PF_5 \rightarrow LiPF_6$ on the samples' mass in DSC measurements.

The secondary thermal phenomena are thus smoother, and the observed exotherm peaks in later cycles are more symmetric and reproducible (Fig. 5). Somewhat similar effects lead to the relative symmetric shapes of the exothermic peaks upon cooling.

The incomplete reformation of $LiPF_6$ upon cooling in the DSC experiments is rationalized on the basis of the necessity of PF_5 to diffuse to the surface of the LiF crystallites through a growing layer of $LiPF_6$ liquid, as discussed in detail for the ARC results. Support for this postulate was adduced by a DSC experiment on a 3.90 mg (25.66 μmol) sample of $LiPF_6$ in which the cooling after heating to 623 K, was extended over 48 h at 473 K, permitting ample time for the reverse reaction. In this case it was found that $LiPF_6$ was reformed to the extent of 95%, rather than the ca. 47% found for the usual experimental conditions.

Only in the cases of samples 1–4 (Fig. 4a) do the DSC (heating) curves clearly show that complete decomposition of the $LiPF_6$ has taken place by 623 K. From the size of the sample in these cases the number of moles of PF_5 produced is available. Assuming the ideal gas law as on approximation, the pressure of PF_5 in the sealed crucible at the temperature of onset of the reverse reaction (reformation of $LiPF_6$) upon cooling (Figs. 4b and 8) was calculated for each of the five samples. The data are plotted in Fig. 9. Extrapolation of the curve to lower pressure indicates that at a PF_5 pressure of 0–1 atm the reformation of $LiPF_6$ should set in below 423 K, below the melting point of $LiPF_6$. Consequently it is now clear why Gavritchev et al. [6] in their experiments involving removal of (most of) gaseous products of decomposition of $LiPF_6$, found upon cooling only one exotherm of $LiPF_6$ reformation (from residual PF_5 in the crucible) at or below ∼421 K, and did not see a separate exotherm for $LiPF_6$ crystallization [6].

From the DSC data, one arrives at an absolute value of ca. 55.8 ± 4.8 kJ mol^{-1} for the internal energy change (ΔU_r) for the decomposition of $LiPF_6$, and of ca. 60.4 ± 7.8 kJ mol^{-1} for its reformation reaction, in the liquid phase (Table 2). The mass of $LiPF_6$, which was formed by the reformation reaction upon cooling (m_{ref}), is equal to: $m_{ref} = Q_{cr}/q_m$, where Q_{cr} is the crystallization heat and q_m the specific melting heat. The specific heat of the reformation reaction (q_{ref}) was estimated as: $q_{ref} = Q_{ref}/m_{ref}$, where Q_{ref} is the heat of the reformation reaction. ΔU_r of $LiPF_6$

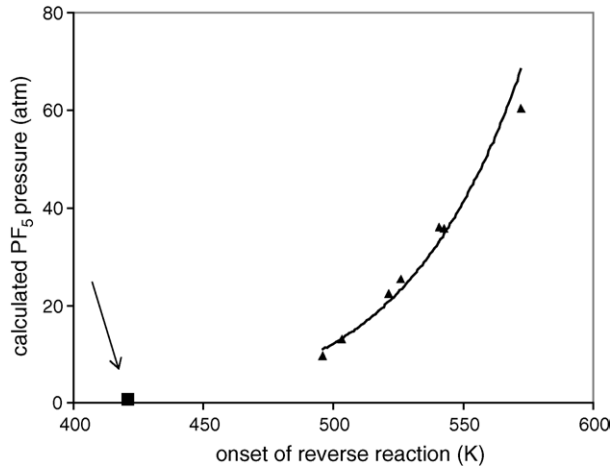

Fig. 9. The calculated PF_5 pressure vs. the onset temperature of the reverse reaction.

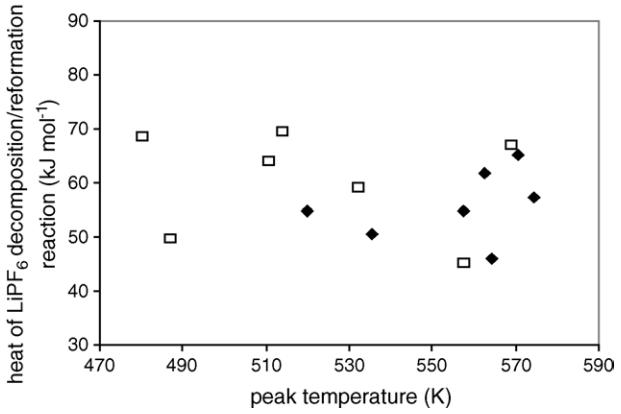

Fig. 10. The heat of $LiPF_6$ decomposition/reformation vs. peak temperature for 7 samples: (♦) heat of decomposition reaction; (□) heat of reformation reaction.

decomposition was calculated approximately as the difference between the total heat related to the endothermic process and the heat of melting.

Fig. 10 presents the values of ΔU_r of decomposition and of reformation of various samples of $LiPF_6$. It may be seen that the value is essentially temperature independent over the range 480–575 K. A similar conclusion was reached above on the basis of ARC measurements over the range (503–578 K).

4. Conclusions

The results of ARC and DSC experiments and their comprehensive analysis demonstrate the reversibility of both the melting of $LiPF_6$ and of its decomposition from liquid state to LiF(s) and PF_5 (g), under conditions of constant volume. The onset of melting is fixed at 466.9 ± 0.3 K, heat of melting is 2.0 ± 0.2 kJ mol^{-1}. Upon cooling crystallization occurs and on exotherm peak onset is observed at 460.9 ± 0.4 K.

Decomposition commences with melting, but in DSC measurements, because of the limiting crucible volume and the pressure of PF_5 produced during decomposition, an increase in the mass of the $LiPF_6$ sample leads to a shift to higher temperature of the peak of the endotherm of decomposition, and of its completion. In the reverse direction, upon cooling, the larger the sample of $LiPF_6$ decomposed, the higher the temperature of onset of reformation of $LiPF_6$ (l) from LiF(s) and PF_5(g). At rates of cooling even as low as 0.5 °C min^{-1}, this reformation reaction is not completed, and the larger the original sample, the more LiF remains after cooling to ambient temperature.

The heat of the endothermic $LiPF_6$ (l) decomposition at constant volume, calculated from the ARC pressure measurements (by a non-calorimetric method using integral form of the van't Hoff isochoric equation), is 64.9 ± 0.3 kJ mol^{-1}. The change in the internal energy for the decomposition and the reformation reactions measured in the DSC experiments is 55.8 ± 4.8 kJ mol^{-1}/60.4 ± 7.8 kJ mol^{-1}, respectively (which allowing for the inherent differences in the techniques and for the approximations in the calculation, is in reasonable agreement with the value derived from ARC). Both ARC and DSC experiments indicate that ΔU_r for $LiPF_6$ decomposition/formation is approximately temperature invariant in the temperature range measured (490–580 K).

References

[1] J. Barthel, J.J. Gores, Handbook of Battery Materials, Wiley-VCH, Weinheim, NY, 1999, p. 457 (Part III, Chapter 7).
[2] D. Aurbach, in: W.A. Van Schalkwijk, B. Scrosati (Eds.), Advances in Li-ion Batteries, Kluwer Academic, Plenum Publishers, NY, London, Moscow, 2002, p. 7 (Chapter 1).
[3] J. Jian, J.R. Dahn, Electrochem. Solid State Lett. 6 (2004) A180.
[4] E.P. Poth, D.H. Goughty, J. Power Sources 128 (2004) 308.
[5] X. Zhang, P.N. Ross Jr., R. Kostecki, F. Kong, S. Sloop, J.B. Kerr, S. Striebel, E.J. Cairns, F. McLarnon, J. Electrochem. Soc. 148 (5) (2001) A463–A470.
[6] K.S. Gavritchev, G.A. Sharpataya, A.A. Smagin, E.N. Malyi, V.A. Matyukha, J. Therm. Anal. Calorim. 73 (2003) 71–83.
[7] K. Tasaki, K. Kanda, S. Nakamura, M. Ue, J. Electrochem. Soc. 150 (12) (2003) A1628–A1636.
[8] G. Gerardine, R. Botte, E. White, Z. Zhang, J. Power Sources 97–98 (2001) 570–575.
[9] A. Du Pasquier, F. Disma, T. Bowmer, A.S. Gozdz, G. Amatucci, J.-M. Tarascon, J. Electrochem. Soc. 145 (2) (1998) 472–477.
[10] D.E. Grey (Ed.), Handbook of the American Institute of Physics, McGraw-Hill, New York, 1972.
[11] jCPDS-ICDD, 82-0784.